Crystal structure and low-temperature behavior of "disordered" thomsonite

G. Diego Gatta,[1,2,*] Volker Kahlenberg,[3] Reinhard Kaindl,[3] Nicola Rotiroti,[1,2] Piergiulio Cappelletti,[4] and Maurizio de' Gennaro[4]

[1]Dipartimento di Scienze della Terra, Università degli Studi di Milano, Via Botticelli 23, I-20133 Milano, Italy
[2]CNR-Istituto per la Dinamica dei Processi Ambientali, Milano, Italy
[3]Institut für Mineralogie und Petrographie, Leopold Franzens Universität Innsbruck, Innrain 52, A-6020 Innsbruck, Austria
[4]Dipartimento di Scienze della Terra, Università Federico II, Via Mezzocannone 8, I-80134 Napoli, Italy

Abstract

The crystal structure, crystal chemistry, and low-temperature structural evolution of natural thomsonite from Terzigno, Somma-Vesuvius volcanic complex, Naples Province, Italy, have been investigated by means of in situ single-crystal X-ray diffraction, electron microprobe analysis in the wavelength dispersive mode, and Raman spectroscopy. Six structure refinements have been obtained at different temperatures: 295.5, 248.0, 198.0, 148.0, 98.0, and 296.0 K (after the low-T experiments). The reflection conditions and the structure refinements prove that the crystal of thomsonite here investigated is orthorhombic with $a = 13.0809(3)$, $b = 13.0597(3)$, $c = 6.6051(1)$ Å, $V = 1128.37(14)$ Å^3, and space group $Pbmn$, which differs from thomsonite from different localities reported in previous studies (with $a \sim 13.1$, $b \sim 13.06$, $c \sim 13.2$ Å, and space group $Pncn$). The refined bond distances suggest that the Si/Al-distribution in the tetrahedral framework is fully "disordered," giving rise to the halving of the c axis relative to that found in "ordered" thomsonites. The extra-framework population consists of: (1) one site about 50% occupied by Ca (labeled as "Ca"); (2) one site occupied by Na (~70%) and Ca (~30%) (labeled as "Na"); and (3) three water molecule sites ("W1," "W2," "W3"). The structure refinements allowed the location of all the proton sites, and the hydrogen-bonding scheme in the structure is provided. The low-temperature refinements show no significant change in the structure within the T-range investigated. The evolution of the unit-cell volume with T exhibits a continuous and linear trend, without any evident thermo-elastic anomaly, with thermal expansion coefficients $\alpha_V = V^{-1} \cdot \partial V / \partial T = 20(2) \cdot 10^{-6}$ K^{-1} (between 98.0 and 295.5 K). A list with the principal Raman active modes is provided and a comparison with the vibrational modes previously found for "ordered" thomsonite is carried out.

Keywords: Zeolite, thomsonite, Somma-Vesuvious, crystal chemistry, low temperature, single-crystal X-ray diffraction, single-crystal Raman spectroscopy

Introduction

Thomsonite is a zeolite belonging to the "fibrous zeolites group," often found in amygdaloidal vugs of massive volcanic rocks (e.g., basalt) and tuffs as an alteration product of volcanic glass (Gottardi and Galli 1985; Armbruster and Gunter 2001; Passaglia and Sheppard 2001; Sheppard and Hay 2001). Thomsonite specimens occur often as spherules or rosettes, composed of platy or blocky crystallites, often associated with gonnardite (Ross et al. 1992). The type locality for this mineral is Old Kilpatrick, near Dumbarton, Scotland (Coombs et al. 1997). The ideal chemical formula of thomsonite is Ca$_2$Na[Al$_5$Si$_5$O$_{20}$]·6H$_2$O ($Z = 4$) (Coombs et al. 1997). Ross et al. (1992) reported an extensive variation in Na/(Ca+Sr) and Si/Al ratio, suggesting that thomsonite compositions lie approximately along the join Na$_4$Ca$_8$Al$_{20}$Si$_{20}$O$_{80}$ and Na$_8$Ca$_4$Al$_{16}$Si$_{24}$O$_{80}$, and that the composition range extends from that of end-member thomsonite, $\square_4$Na$_4$Ca$_8$Al$_{20}$Si$_{20}$O$_{80}$·24H$_2$O, to a composition close to $\square_4$Na$_6$Ca$_6$Al$_{18}$Si$_{22}$O$_{80}$·24H$_2$O, with a general chemical formula $\square_4$Na$_{4+x}$Ca$_{8-x}$[Al$_{20-x}$Si$_{20+x}$O$_{80}$]·24H$_2$O ($Z = 1$), where x varies usu-

ally from about 0 to 2, and $\square$ denotes a cation vacancy in the extra-framework population. Small amounts of Fe, Mg, Sr, Ba, and K also may be found.

The crystal structure of thomsonite was first described by Taylor et al. (1933). The Si/Al tetrahedral framework of thomsonite is built up by 4=1 "secondary building units" (SBU; framework type: THO; Gottardi and Galli 1985; Armbruster and Gunter 2001; Baerlocher et al. 2001) (Fig. 1). The 4=1 units form chains parallel to [001], with tetragonal topological symmetry (Fig. 1). In the THO framework type, the chains form "slices." Within slices perpendicular to the a axis, the SBU chains are not translated relative to one another, whereas within slices perpendicular to the b axis, adjacent SBU chains are mutually translated along [001] by $\pm c/8$ (~1.65 Å; Ross et al. 1992; Gatta 2005). Two different systems of channels occur in the THO framework type: 8-membered ring channels along [001] (hereafter 8mR[001]) and 8-membered ring channels along [010] (hereafter 8mR[010]) (Fig. 1). The topological symmetry of the THO framework type is orthorhombic, with space group $Pmma$ and idealized cell constants: $a = 14.0$, $b = 7.0$, and $c = 6.5$ Å (Baerlocher et al. 2001). Si/Al-ordering and extra-framework content lead to a general symmetry of thomsonite describable with the space group
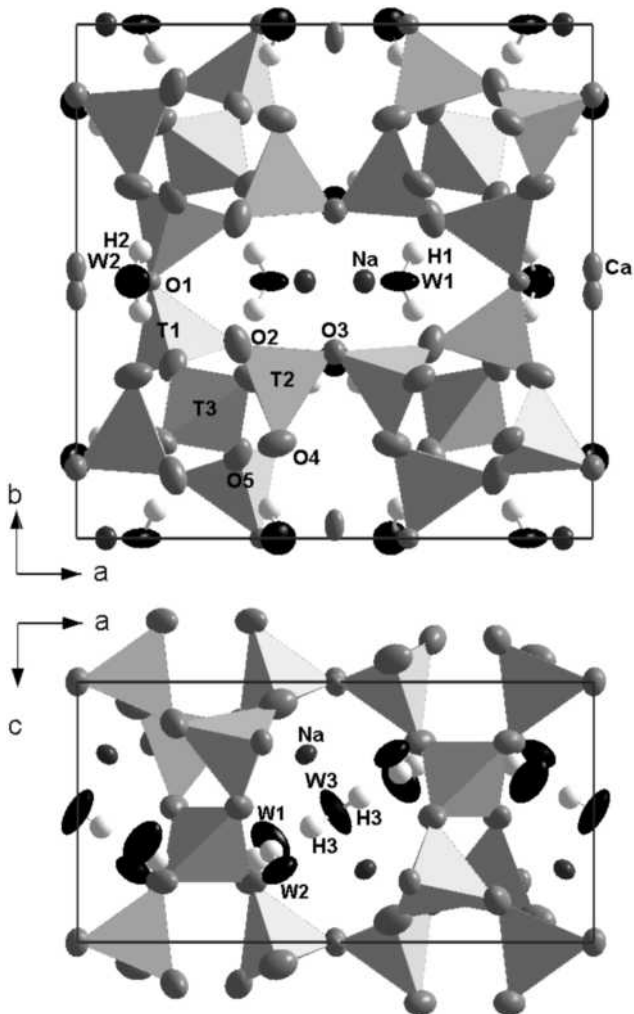
FIGURE 1. The crystal structure of "disordered" thomsonite based on the data reported in this study, (**above**) viewed down [001] and (**below**) down [010]. Thermal ellipsoid probability factor: 99%.

Pncn and *a* ~ 13.09, *b* ~ 13.05, and *c* ~ 13.23 Å (Alberti et al. 1981; Ståhl et al. 1990; Ross et al. 1992). However, a significant number of reflections violating the two *n*-glides found in several experiments (>50; Ståhl et al. 1990; Ross et al. 1992), led Ross et al. (1992) to consider potential different space groups: *Pmc*2_1, *P*2*cm*, or *Pmcm*, rather than *Pncn*.

The Si/Al-distribution in natural thomsonites from several localities have been found as highly ordered (Alberti et al. 1981; Pluth et al. 1985; Ståhl et al. 1990; Ross et al. 1992; Coombs et al. 1997), but evidence of a partial disorder have been reported (Taylor et al. 1933; Amirov et al. 1978). The extra-framework population in the thomsonite structure consists of one site occupied by about 50%Ca, one site partially occupied by Na and Ca, and four independent water molecule sites (Alberti et al. 1981; Pluth et al. 1985; Ståhl et al. 1990; Ross et al. 1992). The structure refinement based on single-crystal neutron diffraction data at 203 (Pluth et al. 1985) and 13 K (Ståhl et al. 1990) provided the positions and the displacement parameters of six independent H sites.

The aim of this study is the investigation of the crystal structure and crystal chemistry of a natural thomsonite specimen,

recently found, in which the *c* axis length is half that found in thomsonites previously reported in the literature. The study was carried out by means of in situ single-crystal X-ray diffraction, electron microprobe analysis in the wavelength dispersive mode (EMPA-WDS) and unpolarized single-crystal Raman spectroscopy. Low-temperature (LT) single-crystal X-ray diffraction data have been collected and LT structure refinements have been obtained to minimize the effects of positional disorder of the extra-framework population.

SAMPLE DESCRIPTION AND MINERALOGY

The sample of thomsonite studied here comes from an ejecta block found in the *Cava Vitiello* quarry in the municipality of Terzigno, Somma-Vesuvius volcanic complex, Naples Province, Italy. The activity of the Somma-Vesuvius volcanic complex started in a submarine environment [first tectonic phase: between the end of Pliocene and the beginning of Pleistocene time; Bernasconi et al. (1981), Santacroce (1987), Brocchini et al. (2001)]. Since that time, the volcanic activity has persisted until today (the last eruption being in 1944) following a cyclic scheme. Each cycle starts with a very powerful explosive "plinian" eruption, followed by a quiescence period of several hundreds of years. Semi-persistent activity continues with minor explosive episodes interspersed with effusive activity and by shorter quiet periods. Lava flows, most of them quite recent in the 1631–1944 activity period [from the first to the seventeenth cycle of the Somma-Vesuvius recent activity; Arnò et al. (1987)], are located just in the southern sector of the complex and originated in the highest slope of the volcano.

From a mineralogical-petrographical point of view, the scientific interest in lava flows from the Somma-Vesuvius complex has always been high, as witnessed by the extensive literature on the subject covering a span of about three centuries [Santacroce (1987) and references therein; Peccerillo (2001) and references therein]. The erupted products range from trachyte to phonolite in composition. Vesuvian lava, also known as *Pietrarsa* ("burned stone"), beginning in the nineteenth century became a fundamental stone in the religious and civil architecture of the town of Naples (Langella et al. 2009).

The physico-chemical conditions favorable to the zeolitization process in vugs of basic volcanic rocks usually produced large and beautiful crystals (*hydrothermal zeolites*). These conditions are mainly due to hydrothermal solutions, in connection with late stages of magma crystallization. Nonetheless, favorable conditions could also be related to interactions of hot ascending fluids within the host rocks, through joints and fractures in places where the thermal fluids are at high temperature and thus able to leach ions. These solutions, once temperature decreases, gave birth in open spaces and cavities to zeolites and other minerals.

The presence of thomsonite among the Vesuvian zeolites, described as white globular radiating masses found in amygdaloidal vugs, was previously reported by Russo (1999) and confirmed by the late E. Franco (Russo and Punzo 2004). Russo (1999) also reported the presence of acicular crystals of thomsonite, with other fibrous zeolites (e.g., gonnardite), in zeolitized ejecta, but no crystallographic and crystal-chemical data of this mineral from the Somma-Vesuvius complex have been so far reported.

EXPERIMENTAL METHODS

Thomsonite represents the main zeolitic mineral of the sample. Among the large number of crystals investigated, only a few single crystals of thomsonite showed the halving of the c axis (i.e., with $a \sim 13.08$, $b \sim 13.06$, and $c \sim 6.6$ Å), and only one with a size appropriate for a single-crystal X-ray diffraction experiment ($\sim 130 \times 100 \times 50$ μm), suitable for a structural refinement, was found. A few other small crystals ($\sim 25 \times 15 \times 10$ μm), with similar unit-cell parameters, were selected for the microprobe analysis.

Quantitative EMPA-WDS analyses were performed on two polished single crystals using a Jeol JXA-8200 electron microprobe. The system was operated using a defocused electron beam (∅ 5 μm), an accelerating voltage of 15 kV, a beam current of 10 nA measured by a Faraday cup, and counting times of 20 s on the peaks and 5 s on the backgrounds. This protocol was aimed to reduce dehydration or cation migration under the electron beam. Natural crystals of K-feldspar (for Si, K, Al), wollastonite (for Ca), barite (for Ba), celestine (for Sr), omphacite (for Na), and forsterite (for Mg) were used as standards; H_2O fraction was calculated by difference. The results were corrected for matrix effects using a conventional ZAF routine in the Jeol suite of programs. The crystals were found to be chemically homogeneous. Despite the very small dimensions of the crystals, consistent chemical analyses (obtained by averaging 6 point analyses and calculated on the basis of 80 O atom) were obtained. The chemical formula of one of the two crystals was $Na_{7.54}Ca_{5.37}[Al_{17.15}Si_{22.56}]_{\Sigma=39.71}O_{80} \cdot 26.2H_2O$, which would be considered gonnardite (or tetranatrolite) rather than thomsonite (with $a \sim b \sim 13.1$ and $c \sim 6.6$ Å; Mazzi et al. 1986; Ross et al. 1992; Artioli and Galli 1999; Evans et al. 2000). For the other small crystal, the resultant chemical formula was $K_{0.03}Na_{4.33}Ca_{5.85}Mg_{0.52}[Al_{16.81}Si_{23.12}]_{\Sigma=39.93}O_{80} \cdot 23.6H_2O$, which could be considered as Ca-poor thomsonite.

Intensity diffraction data were collected at 295.5, 248.0, 198.0, 148.0, 98.0, and 296.0 K (after the low-T experiments) using an Oxford Diffraction Gemini diffractometer equipped with a Ruby CCD detector and graphite monochromated Mo$K\alpha$ radiation (Enhance X-ray optics) operating at 50 kV and 40 mA. For the low-temperature data sets, the crystal was slow-cooled with an Oxford Cryosystems 700 open-flow nitrogen gas system (temperature stability better than 0.2 K and absolute uncertainty in temperature at the crystal position <2 K). All the data collections were performed using a combination of ω and φ scans to maximize the reciprocal space coverage and redundancy, with an exposure time of 30 s per frame (Table 1). The diffraction patterns within the T range investigated show a metrically orthorhombic lattice, with $a = 13.0809(3)$, $b = 13.0597(3)$, $c = 6.6051(1)$ Å, and $V = 1128.37(14)$ Å^3. The indexing was done maintaining the metrics of the thomsonite lattice on (001), with $a > b$. No evidence of non-merohedral twinning was found. Lorentz-polarization and analytical absorption corrections, by Gaussian integration based upon the physical description of the crystal (CrysAlis, Oxford
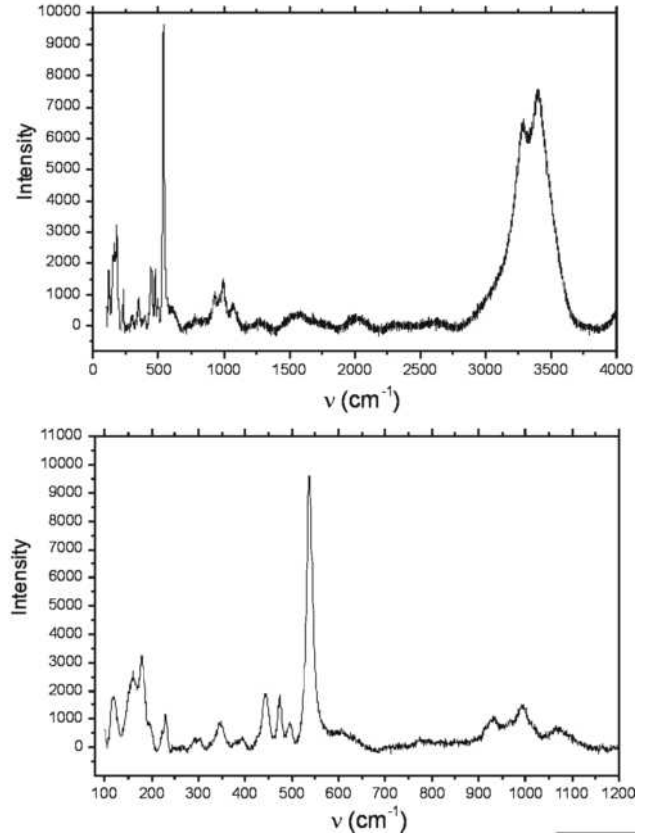

FIGURE 2. Unpolarized single-crystal Raman spectrum of "disordered" thomsonite collected at room conditions in the region from 100 to 4000 cm^{-1} (**above**) and the region from 100 and 1200 cm^{-1} (**below**). The list with the frequencies of the main Raman bands is given in Table 5. Both spectra are background-corrected.

TABLE 1. Details of data collection and refinement of "disordered" thomsonite at different temperatures

T (K)	295.5	248.0	198.0	148.0	98.0	296.0*
a (Å)	13.0809(3)	13.0791(3)	13.0717(3)	13.0643(3)	13.0603(3)	13.0827(3)
b (Å)	13.0597(3)	13.0581(3)	13.0527(4)	13.0492(4)	13.0456(3)	13.0588(3)
c (Å)	6.6051(1)	6.6046(2)	6.6007(2)	6.6002(2)	6.5981(2)	6.6071(1)
V (Å^3)	1128.37(14)	1127.99(5)	1126.22(5)	1125.19(5)	1124.18(5)	1128.79(4)
Space group	Pbmn	Pbmn	Pbmn	Pbmn	Pbmn	Pbmn
Radiation	Mo$K\alpha$	Mo$K\alpha$	Mo$K\alpha$	Mo$K\alpha$	Mo$K\alpha$	Mo$K\alpha$
Detector type	CCD	CCD	CCD	CCD	CCD	CCD
Scan type	ω/φ	ω/φ	ω/φ	ω/φ	ω/φ	ω/φ
Scan width (°)	1.5	1.5	1.5	1.5	1.5	1.5
Exposure time (s)	30	30	30	30	30	30
2θ max (°)	~60	~60	~60	~60	~60	~60
	−15≤h≤17	−17≤h≤14	−17≤h≤14	−15≤h≤17	−14≤h≤17	−15≤h≤17
	−10≤k≤16	−16≤k≤10	−16≤k≤10	−14≤k≤17	−11≤k≤16	−11≤k≤16
	−8≤l≤8	−8≤l≤8	−8≤l≤8	−7≤l≤8	−8≤l≤8	−8≤l≤8
Coverage	99.7%	99.7%	99.7%	99.7%	99.7%	99.7%
No. measured reflections	7423	7151	7084	7087	7020	7173
No. unique reflections	1351	1374	1380	1367	1359	1355
No. unique reflections with $F_o > 4\sigma(F_o)$	1167	1167	1132	1184	1168	1142
No. refined parameters	119	119	119	119	119	119
R_{int}	0.0301	0.0310	0.0348	0.0300	0.0314	0.0311
R_1 (F) with $F_o > 4\sigma(F_o)$	0.0242	0.0222	0.0237	0.0225	0.0220	0.0231
wR_2 (F^2)	0.0465	0.0435	0.0442	0.0428	0.0426	0.0459
GooF	1.192	1.122	1.065	1.133	1.116	1.149
Residuals (e^-/Å^3)	+0.38/−0.40	+0.45/−0.27	+0.31/−0.27	+0.42/−0.31	+0.34/−0.31	+0.46/−0.45

Note: $R_{int} = \Sigma|F_{obs}^2 - F_{obs}^2(\text{mean})|/\Sigma(F_{obs}^2)$; $R_1 = \Sigma(|F_{obs}| - |F_{calc}|)/\Sigma|F_{obs}|$; $wR_2 = \{\Sigma[w(F_{obs}^2 - F_{calc}^2)^2]/\Sigma[w(F_{obs}^2)^2]\}^{0.5}$, $w = 1/[\sigma^2(F_{obs}) + (0.02*P)^2]$, $P = [\text{Max}(F_{obs}^2, 0) + 2*F_{calc}^2]/3$.
* Data collected at room conditions after the low-T experiment.

Diffraction 2009), were performed. The discrepancy factors between symmetry related diffraction intensities (Laue class *mmm*) are listed in Table 1.

A single-crystal Raman spectrum was collected at room conditions from the same crystal recovered from the X-ray diffraction experiments, using a microscope attached to a Jobin-Yvon Labram-HR800 confocal micro-Raman spectrometer equipped with a charge-coupled detector (CCD). The sample was excited with an Ar^+ laser (30mW, 488nm). The unpolarized laser beam was focused through a 100× objective (N.A. = 0.9) to a 1 μm spot on the sample. Laser power at the sample surface was ~1 mW. The range from 100 to 4000 cm^{-1} was investigated, with spectral resolution below 2 cm^{-1} and collected in backscattered geometry (Fig. 2). Accuracy of Raman line shifts, calibrated by regular measuring of the Rayleigh line, was in the order of 0.5 cm^{-1}.

RESULTS

Structure refinements at different temperatures

The intensity data for thomsonite collected at 295.5 K were first processed with the programs E-STATISTICS and ASSIGN-SPACEGROUP, implemented in the WinGX package (Farrugia 1999), in order to provide the Wilson plot, the normalized structure factors (*E* values) and the statistics of their distributions, and the most likely space group. The structure was found to be centrosymmetric at 94.63% likelihood, in agreement with the results of Sheldrick's $|E^2–1|$ criterion (Sheldrick 1997) ($|E^2–1| = 0.949$). Two possible space groups have been suggested, *Pb2n* and *Pbmn*.

The anisotropic structure refinement based on the data collected at 295.5 K was performed using the SHELX-97 software (Sheldrick 1997), starting from the structural model of the ideal THO framework type rearranged in the space group *Pbmn*. Neutral atomic scattering factors for Na, Ca, Al, Si, O, and H were taken from the *International Tables for Crystallography* (Wilson and Prince 1999). Correction for secondary isotropic extinction was not necessary. After the first cycles of refinement, the maxima in the difference-Fourier maps of the electron density allowed the location of the extra-framework population (Fig. 1; Table 2). The refined tetrahedral bond distances showed a highly disordered Si/Al-distribution (Table 3a). However, a scattering curve based on partially occupied tetrahedral sites by Al and Si did not significantly improve the figures of merit of the refinement. The Ca site was located at the special position 1/2, ~0.0242, 0 with partial site occupancy, and was modeled to be occupied exclusively by Ca. Using a mixed (Ca+Na) scattering curve, the refinement led to a non-significant amount of Na. In addition, the Ca scattering curve alone led to a site occupancy factor close to 50%, which is the maximum value in this structure model (Fig. 1; Table 2). A mixed scattering curve was used for the Na site, and the best fit was achieved with (~30% Ca + ~70% Na). A careful inspection of the difference-Fourier

TABLE 2. Refined positional and thermal displacement parameters (Å^2) of "disordered" thomsonite at 295.5 and 98.0 K

T = 295.5 K

Site	Occ.	x	y	z	U_{11}	U_{22}	U_{33}	U_{12}	U_{13}	U_{23}	U_{eq}/U_{iso}
Ca	0.473(2)	1/2	0.02423(6)	0	0.0096(4)	0.0247(10)	0.0088(4)	0	0.0015(3)	0	0.0144(4)
Na	Na 0.700(6) Ca 0.300(6)	0.05755(4)	0	0.27736(9)	0.0127(4)	0.0152(4)	0.0126(4)	0	0.0019(3)	0	0.0135(3)
T1	1	0.30886(3)	0.11926(3)	0.24134(6)	0.0069(2)	0.0094(3)	0.0067(2)	0.00102(15)	0.00009(16)	–0.00018(15)	0.0077(2)
T2	1	0.11609(3)	0.19516(3)	0.00259(6)	0.0080(2)	0.0076(2)	0.0075(2)	–0.00156(15)	0.00091(16)	–0.00033(15)	0.0077(2)
T3	1	1/4	1/4	0.62085(8)	0.0078(3)	0.0074(3)	0.0057(3)	–0.0009(2)	0	0	0.0070(2)
O1	1	0.35599(10)	0	0.2320(2)	0.0103(6)	0.0099(7)	0.0146(8)	0	0.0009(6)	0	0.0116(3)
O2	1	0.18715(7)	0.12254(8)	0.15831(16)	0.0133(5)	0.0291(7)	0.0181(6)	–0.0030(5)	0.0000(4)	–0.0022(5)	0.0202(3)
O3	1	0	0.13831(10)	0	0.0102(6)	0.0124(7)	0.0158(8)	0	–0.0002(6)	0	0.0128(3)
O4	1	0.38882(7)	0.18394(8)	0.08666(16)	0.0266(6)	0.0148(6)	0.0194(6)	0.0027(5)	–0.0018(5)	0.0016(4)	0.0203(3)
O5	1	0.31168(8)	0.16259(8)	0.48011(15)	0.0182(5)	0.0225(6)	0.0136(6)	0.0048(4)	0.0006(4)	0.0017(5)	0.0181(3)
O6	1	0.16322(7)	0.19105(8)	0.76725(15)	0.0207(6)	0.0169(6)	0.0132(6)	–0.0061(4)	0.0012(4)	–0.0007(4)	0.0169(3)
W1	0.952(8)	0.12651(14)	0	0.6214(3)	0.0343(12)	0.0111(12)	0.0449(14)	0	–0.0140(9)	0	0.0301(7)
W2	0.966(8)	0.39281(14)	0	0.7218(3)	0.0355(11)	0.0276(13)	0.0216(11)	0	–0.0137(8)	0	0.0282(7)
W3	0.912(8)	0	0.15299(16)	1/2	0.0227(11)	0.0279(13)	0.0395(14)	0	–0.0162(9)	0	0.0300(8)
H1	1	0.1557(17)	0.0552(18)	0.678(4)							0.069(8)
H2	1	0.3776(17)	0.0600(17)	0.652(4)							0.067(8)
H3	1	0.0426(19)	0.1975(19)	0.557(4)							0.081(9)

T = 98.0 K

Site	Occ.	x	y	z	U_{11}	U_{22}	U_{33}	U_{12}	U_{13}	U_{23}	U_{eq}/U_{iso}
Ca	0.474(2)	1/2	0.02656(5)	0	0.0048(4)	0.0096(7)	0.0034(4)	0	0.0004(3)	0	0.0059(3)
Na	Na 0.676(6) Ca 0.324(6)	0.05752(4)	0	0.27934(8)	0.0069(3)	0.0073(4)	0.0056(3)	0	0.0010(2)	0	0.0066(3)
T1	1	0.30955(3)	0.11932(3)	0.24222(5)	0.0048(2)	0.0071(2)	0.0041(2)	0.00086(14)	–0.00012(14)	–0.00046(15)	0.0053(1)
T2	1	0.11617(3)	0.19432(3)	0.00348(6)	0.0058(2)	0.0045(2)	0.0044(2)	–0.00081(14)	0.00119(14)	–0.00049(14)	0.0049(1)
T3	1	1/4	1/4	0.62166(8)	0.0049(3)	0.0042(3)	0.0037(3)	–0.0006(2)	0	0	0.0043(2)
O1	1	0.35713(9)	0	0.23256(18)	0.0064(6)	0.0080(7)	0.0085(7)	0	0.0006(5)	0	0.0076(3)
O2	1	0.18719(7)	0.12228(8)	0.16066(14)	0.0109(5)	0.0206(6)	0.0116(5)	–0.0034(4)	0.0021(4)	–0.0041(4)	0.0144(3)
O3	1	0	0.13719(10)	0	0.0077(6)	0.0101(7)	0.0110(7)	0	–0.0001(5)	0	0.0096(3)
O4	1	0.38882(7)	0.18421(8)	0.08607(14)	0.0211(5)	0.0106(6)	0.0126(6)	0.0030(4)	–0.0035(4)	–0.0011(4)	0.0147(3)
O5	1	0.31316(7)	0.16315(8)	0.48127(13)	0.0105(4)	0.0146(6)	0.0094(5)	0.0015(4)	0.0001(4)	0.0035(4)	0.0114(2)
O6	1	0.16354(7)	0.18953(8)	0.76774(13)	0.0145(5)	0.0100(6)	0.0083(5)	–0.0030(4)	–0.0005(4)	–0.0012(4)	0.0109(2)
W1	0.947(8)	0.12617(11)	0	0.6206(2)	0.0183(9)	0.005(1)	0.0249(10)	0	–0.0079(7)	0	0.0161(6)
W2	0.979(8)	0.39103(11)	0	0.7239(2)	0.0153(8)	0.0121(11)	0.0098(9)	0	–0.0050(6)	0	0.0124(6)
W3	0.923(8)	0	0.15273(13)	1/2	0.0135(9)	0.0118(10)	0.0257(11)	0	–0.0124(7)	0	0.0170(6)
H1	1	0.1551(15)	0.0571(16)	0.677(3)							0.047(6)
H2	1	0.3736(14)	0.0561(15)	0.653(3)							0.040(6)
H3	1	0.0396(15)	0.1951(16)	0.561(3)							0.042(6)

Notes: The anisotropic displacement factor exponent takes the form: $–2\pi^2[(ha^*)^2U_{11} +...+ 2hka^*b^*U_{12}]$. U_{eq} is defined as one third of the trace of the orthogonalized U_{ij} tensor. For the T1, T2, and T3 sites, the scattering curve of neutral Si was used. The refined numbers of electrons per site (<14 e^-) show the presence of Al for all the T1, T2, and T3 sites. For the Ca site, the scattering curve of Ca was used, whereas for the Na site a mixed scattering curve (Na+Ca) was adopted.

maps of the electron density allowed location of all the H sites (Fig. 1; Table 2). The last cycles of refinement were conducted after the location of the proton positions, and convergence was rapidly achieved. The variance-covariance matrix did not show any significant correlations among the refined parameters. The residual electron density in the difference-Fourier map at the end of the refinement varied between +0.38 and –0.40 e^-/Å^3, with an agreement factor $R_1(F) = 0.0242$ based on 1167 unique reflections with $F_o > 4\sigma(F_o)$ and 119 refined parameters (Table 1).

The space group assignment and structure refinements based on the intensity data collected at low T were carried out using the same protocol and the refined structural model for the 295.5 K structure. The symmetry and the general structure configuration are maintained within the T-range investigated. Further details pertaining to the refinements are reported in Table 1. Atomic positions and anisotropic thermal displacement parameters at 295.5 and 98.0 K are listed in Table 2. Refined bond distances and angles at 295.5 and 98.0 K are listed in Tables 3a and 3b, respectively. For the refinements at 248.0, 198.0, 148.0, and 296.0 K (after the low-T experiments), positional parameters, atomic displacement parameters, bond distances and angles are deposited (Table 4[1]).

Raman spectrum

In the spectral range investigated in this study, 24 bands are distinguishable. These are designed υ_1 to υ_{24} with increasing wavenumber and listed in Table 5. For some regions of the spectrum, a fit with two Lorentzian profiles was used to resolve overlapping peaks.

According to previous Raman spectroscopic investigations of fibrous zeolites (Dutta and Del Barco 1985; Dutta and Puri 1987; Gillet et al. 1996; Wopenka et al. 1998, and references therein), the following general mode assignments can be outlined. The modes between 3000–3800 cm^{-1} are caused by O-H stretching modes of extra-framework water molecules. The modes between 900 and 1100 cm^{-1} are assigned to inter-tetrahedral anti-symmetric T-O-T (T = Si or Al) stretching vibrations. Inter-tetrahedral symmetric T-O-T stretching vibrations range between 660 and 760 cm^{-1}. The modes with frequencies below 550 cm^{-1} are assigned to various intra-tetrahedral δ(O-T-O) bending and rotational modes, and to lattice modes. The most intense mode near 540 cm^{-1} can be attributed to motion of the O atom in the plane perpendicular to the T-O-T bond (Dutta and Del Barco 1985; Dutta and Puri 1987; Gillet et al. 1996; Wopenka et al. 1998) and appears to be a common feature for all fibrous zeolites.

TABLE 3a. Relevant bond distances (Å) and angles (°) in the "disordered" thomsonite structure at 295.5 K

Ca-Ca*	0.633(1)	T2-O6†	1.673(1)	O5-T1-O1	109.89(4)
Ca-W2†	2.333(2)	T2-O4††	1.675(1)	O5-T1-O2	108.58(5)
Ca-W2‡	2.333(2)	T2-O2	1.680(1)	O1-T1-O2	111.06(4)
Ca-O1	2.449(1)	T2-O3	1.690(1)	O5-T1-O4	112.76(5)
Ca-O1*	2.449(1)	<T2-O>	1.6795	O1-T1-O4	102.40(4)
Ca-O4§	2.606(1)			O2-T1-O4	112.07(5)
Ca-O4	2.606(1)	T3-O6††	1.678(1)		
		T3-O6	1.678(1)		
Na-W1	2.445(2)	T3-O5	1.679(1)	O6†-T2-O4††	110.63(5)
Na-O2	2.460(1)	T3-O5††	1.679(1)	O6†-T2-O2	110.30(5)
Na-O2‖	2.460(1)	<T3-O>	1.6785	O4††-T2-O2	110.52(5)
Na-W1#	2.499(2)			O6†-T2-O3	107.91(4)
Na-W3#	2.593(2)	W1-H1	0.897(24)	O4††-T2-O3	112.52(4)
Na-W3	2.593(2)	W1⋯O6	2.717(1)	O2-T2-O3	104.79(4)
Na-O3**	2.681(1)	H1⋯O6	1.873(24)		
Na-O3	2.681(1)	H1-W1-H1	107(2)		
		W1-H1⋯O6	156(2)	O6††-T3-O6	109.63(5)
				O6††-T3-O5	107.81(5)
T1-O5	1.676(1)	W2-H2	0.931(23)	O6-T3-O5	109.40(5)
T1-O1	1.676(1)	W2⋯O5	2.861(2)	O6††-T3-O5††	109.40(5)
T1-O2	1.684(1)	H2⋯O5	1.955(23)	O6-T3-O5††	107.81(5)
T1-O4	1.689(1)	H2-W2-H2	115(2)	O5-T3-O5††	112.75(5)
<T1-O>	1.6812	W2-H2⋯O5	163(2)		
		W3-H3	0.889(25)		
		W3⋯O6	2.815(1)		
		H3⋯O6	2.106(25)		
		H3-W3-H3	99(2)		
		W3-H3⋯O6	136(2)		

Notes: The possible H-bond configurations are given. Symmetry codes:
* 1–x, –y, –z;
† x, y, –1+z
‡ 1–x, –y, 1–z
§ 1–x, y, –z
‖ x, –y, z
–x, –y, 1–z;
** –x, –y, –z;
†† 0.5–x, 0.5–y, z
‡‡ –x, y, –z
§§ x, y, 1+z.

TABLE 3b. Relevant bond distances (Å) and angles (°) in the "disordered" thomsonite structure at 98.0 K

Ca-Ca*	0.693(1)	T2-O6†	1.675(1)	O1-T1-O5	109.97(4)
Ca-W2†	2.338(1)	T2-O4††	1.677(1)	O1-T1-O2	111.11(4)
Ca-W2‡	2.338(1)	T2-O2	1.679(1)	O5-T1-O2	108.58(5)
Ca-O1	2.441(1)	T2-O3	1.691(1)	O1-T1-O4	102.41(4)
Ca-O1*	2.441(1)	<T2-O>	1.6805	O5-T1-O4	112.67(5)
Ca-O4§	2.581(1)			O2-T1-O4	112.01(5)
Ca-O4	2.581(1)	T3-O5	1.680(1)		
		T3-O5††	1.680(1)		
Na-W1	2.424(1)	T3-O6††	1.681(1)	O6†-T2-O4††	110.57(5)
Na-O2	2.455(1)	T3-O6	1.681(1)	O6†-T2-O2	110.40(5)
Na-O2‖	2.455(1)	<T3-O>	1.6805	O4††-T2-O2	110.47(5)
Na-W1#	2.488(2)			O6†-T2-O3	107.60(4)
Na-W3**	2.580(1)	W1-H1	0.914(20)	O4††-T2-O3	112.71(4)
Na-W3	2.580(1)	W1⋯O6	2.701(1)	O2-T2-O3	104.92(4)
Na-O3#	2.677(1)	H1⋯O6	1.832(21)		
Na-O3	2.677(1)	H1-W1-H1	109(2)		
		W1-H1⋯O6	158(2)	O5-T3-O5††	113.07(5)
				O5-T3-O6††	107.63(5)
T1-O1	1.677(1)	W2-H2	0.898(20)	O5††-T3-O6††	109.24(4)
T1-O5	1.678(1)	W2⋯O5	2.851(1)	O5-T3-O6	109.24(4)
T1-O2	1.687(1)	H2⋯O5	1.963(20)	O5††-T3-O6	107.63(5)
T1-O4	1.688(1)	H2-W2-H2	109(2)	O6††-T3-O6	110.04(5)
<T1-O>	1.6825	W2-H2⋯O5	169(2)		
		W3-H3	0.857(20)		
		W3⋯O6	2.813(1)		
		H3⋯O6	2.118(20)		
		H3-W3-H3	100(2)		
		W3-H3⋯O6	138(2)		

Notes: The possible H-bond configurations are given. Symmetry codes:
* 1–x, –y, –z;
† x, y, –1+z;
‡ 1–x, –y, 1–z;
§ 1–x, y, –z;
‖ x, –y, z;
–x, –y, 1–z;
** –x, –y, –z;
†† 0.5–x, 0.5–y, z;
‡‡ –x, y, –z;
§§ x, y, 1+z.

TABLE 5. Frequencies of Raman bands of "disordered" thomsonite at room conditions

Bands	Frequency (cm^{-1})
ν_1	119
ν_2	160
ν_3	179
ν_4	195
ν_5	224
ν_6	230
ν_7	294
ν_8	304
ν_9	347
ν_{10}	383
ν_{11}	395
ν_{12}	430
ν_{13}	444
ν_{14}	474
ν_{15}	495
ν_{16}	537
ν_{17}	606
ν_{18}	774
ν_{19}	930
ν_{20}	966
ν_{21}	993
ν_{23}	1069
ν_{24}	3278
ν_{25}	3420

DISCUSSION AND CONCLUSIONS

The crystal structure of thomsonite with a fully "disordered" Si/Al-distribution in the tetrahedral framework (Tables 3a, 3b, and 4) is here described on the basis of high-quality anisotropic structural refinements, with the location of all the proton sites. The disorder gives rise to the halving of the c axis relative to that found in "ordered" thomsonites (i.e., in "ordered" thomsonite c ~ 13.2 Å, and in "disordered" thomsonite c ~ 6.6 Å). The extra-framework population consists of one site partially occupied by Ca (Ca site), a further cationic site occupied by Na and Ca (Na site) and three independent water molecule sites (W1, W2, W3, H1, H2, H3). The coordination shell of the Na site is a large and distorted polyhedron with coordination number CN = 8 (four framework O atoms + four H$_2$O molecules) (Tables 3a, 3b, and 4). The coordination shell of the Ca site consists of a distorted octahedra (CN = 6) (four framework O atoms + two H$_2$O molecules, Tables 3a, 3b, and 4). Despite the weak X-ray scattering factor of hydrogen, the geometrical configuration of the water molecules and the H-bonding scheme found in "disordered" thomsonite structure are consistent (Fig. 3; Tables 3a, 3b, and 4). The geometry of the molecules is better described

at low T, as shown in particular by the H-O-H angles. Only for the water molecules labeled as W3 do the W3-H3···O6 angles refined at all temperatures (~140°, Tables 3a, 3b, and 4) appear to be significantly low, although still in the range of the observed ones in this class of materials (Chiari and Ferraris 1982; Steiner 1998; Gatta et al. 2008; Della Ventura et al. 2009).

The unit-formula based on the structure refinement at room temperature is: $^{Na,Ca}(Na_{5.68}Ca_{6.08})^T(Al,Si)_{\Sigma=40}O_{80} \cdot 22.64H_2O$ (Z = 0.5), which is significantly, but not drastically, different with respect to the EMPA-WDS results [i.e., $K_{0.03}Na_{4.33}Ca_{5.85}Mg_{0.52}$ $[Al_{16.81}Si_{23.12}]_{\Sigma=39.93}O_{80} \cdot 23.6H_2O$]. We cannot exclude that the differences about the extra-framework cations could be due to some K at the Ca site, here refined using only the Ca scattering curve, and to Mg at the Na site. This would explain the higher amount of Ca and Na obtained by the structure refinement than with the chemical analysis. The total number of electrons of the two extra-framework cation sites, calculated on the basis of the structure refinement, and that obtained on the basis of the chemical analysis, differ by 6.8%, and are, respectively, $\Sigma e^-_{(Ca+Na\ site)}$ = 184.1 e^- and $\Sigma e^-_{(Ca+Mg+Na+K)}$ = 171.5 e^-. However, the chemical analysis was based on data collected from a different crystallite than that used for the structure refinements, and this would be a potential source of the differences, coupled with water and Na migration under the electron beam of the microprobe.

Comparison between the refinements at different temperatures shows that no significant variation in the configuration of framework and extra-framework content occurs within the T-range investigated. In contrast, some other zeolites show low-T induced rearrangements of the extra-framework population (Rotiroti et al. 2008; Gatta et al. 2009). It is interesting to note how the low-T conditions appear to lead to a structural evolution of the framework opposite to that observed in response to high pressure. Gatta (2005, 2008) showed that the response of all the fibrous zeolites compressed under hydrostatic conditions is represented by the cooperative rotation of the 4=1 SBU around the SBU-axis (i.e., [001]). Such a mechanism leads to a significant decrease of the two acute O-O-O angles of the 8mR[001], coupled with an increase of the two (most) obtuse O-O-O angles of the ring. Low T seems to activate an opposite mechanism, with a drastically lower magnitude. In fact, the O2-O3-O2 angle is 171.65(3)° at 295.5 K and slightly decreases to 171.15(3)° at 98.0 K, whereas a slight increase of the O2-O1-O2 angle from 70.20(3) at 295.5 K to 70.57(3)° at 98.0 K occurs.
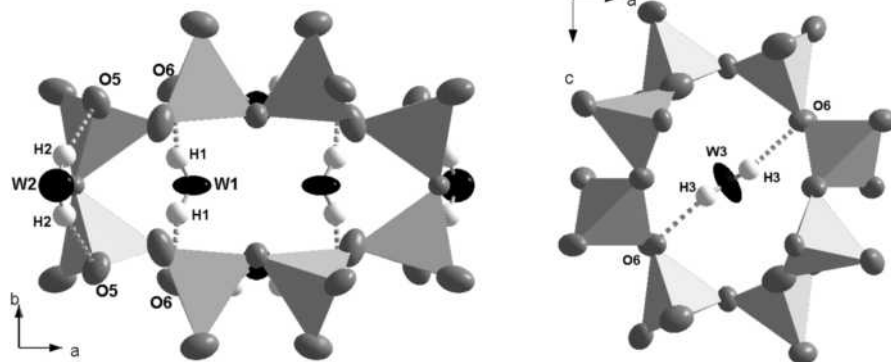

◄**FIGURE 3.** Configuration of the H-bonds in "disordered" thomsonite at 98 K. Thermal ellipsoid probability factor: 99%.
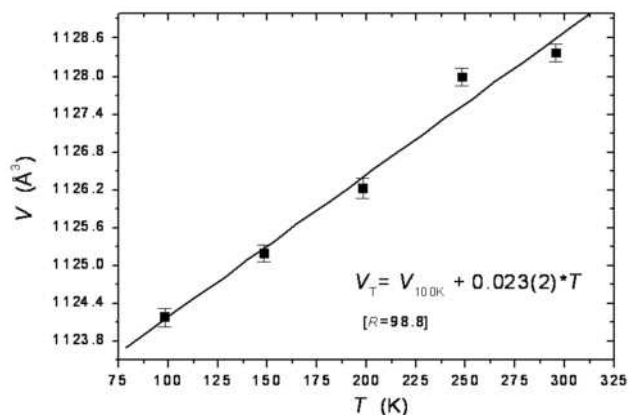
FIGURE 4. Evolution of the unit-cell volume of "disordered" thomsonite with T. The weighted linear regression through the data points is shown.

The variation of the unit-cell volume of "disordered" thomsonite as a function of T is shown in Figure 4. The trend is continuous and linear, without any thermo-elastic anomaly within the T-range investigated. The volume thermal expansion coefficients ($\alpha_V = V^{-1} \cdot \partial V/\partial T$) between 98.0 and 295.5 K was calculated by weighted linear regression through the data points, yielding $\alpha_V = 20(2) \cdot 10^{-6}$ K^{-1}.

The Raman spectrum of "disordered" thomsonite shows strong similarities with that of "ordered" thomsonite reported by Wopenka et al. (1998), who assigned 38 Raman active modes between 100–4000 cm^{-1}. The spectrum that we collected shows two intense vibrational modes active in the O-H stretching region, at 3278 (υ_{23}) and 3420 (υ_{24}) cm^{-1}, respectively (Table 5). No significantly intense Raman active band due to the bending mode of water was found. Three intense bands at 966 (υ_{20}), 993 (υ_{21}), and 1069 (υ_{24}) cm^{-1} are assigned to inter-tetrahedral anti-symmetric T-O-T stretching vibrations (Table 5). For the "ordered" thomsonite, the corresponding bands were found at 977, 988, and 1072 cm^{-1}, respectively (Wopenka et al. 1998). Inter-tetrahedral symmetric T-O-T stretching vibrations, ranging between 660 and 760 cm^{-1}, are represented only by weak bands in both "ordered" and "disordered" thomsonite (Fig. 2; Table 5; Wopenka et al. 1998). The most intense band of the spectrum, pertaining to the low-energy δ(O-T-O) bending mode, was found at 533 cm^{-1} for "ordered" thomsonite (Wopenka et al. 1998), and at 538 cm^{-1} (υ_{16}) for the "disordered" form (Table 5). Further significantly intense bands assignable to δ(O-T-O) bending modes were found at 449 and 475 cm^{-1} in "ordered" thomsonite, and at 444 and 474 cm^{-1} in the "disordered" one (υ_{13}).

The crystal identification of "disordered" thomsonite is not easy. Considering only the unit-cell parameters ($a \sim 13.08$, $b \sim 13.06$, $c \sim 6.6$ Å), one would be driven to ascribe the crystal to gonnardite (or tetranatrolite) ($a \sim b \sim 13.1$, $c \sim 6.6$ Å; Mazzi et al. 1986; Ross et al. 1992; Artioli and Galli 1999; Evans et al. 2000). Furthermore, the chemical analysis does not always provide a unique answer, because of the extensive variation in Na/Ca and Si/Al ratios in thomsonite toward chemical compositions close to that of gonnardite (Ross et al. 1992). Similarly, the unpolarized single-crystal Raman spectrum would also lead to an ambiguous identification among (Ca+Na)-bearing fibrous zeolites. Only the

structure refinement can prove, unambiguously, the nature of the crystal, as the structure of gonnardite, for example, consists of NAT framework type, and not THO as in thomsonite (Baerlocher et al. 2001). A further source of confusion is the structural model of "orthorhombic gonnardite" reported by Amirov et al. (1972), which is more likely "disordered" thomsonite rather than gonnardite, as shown by the THO framework type deducible from the structural data.

The occurrence of two forms of thomsonite in nature, i.e., "ordered" (with $c \sim 13.2$ Å) and "disordered" (with $c \sim 6.6$ Å), is not easily ascribable to different stability fields, as for proper polymorphs. A similar finding has been reported for other fibrous zeolites, e.g., edingtonite. Gatta et al. (2004a, 2004b) and Gatta and Boffa Ballaran (2004) reported the occurrence of coexisting orthorhombic ($P2_12_12$) and tetragonal ($P\overline{4}2_1m$) edingtonite in a sample from Ice River, on the basis of X-ray single-crystal diffraction data. The crystals of the two modifications were adjacent, without any evidence of intergrowth. The main difference between the two forms is the different Si/Al-distribution in the tetrahedral framework: completely "ordered" in orthorhombic edingtonite and completely "disordered" in tetragonal edingtonite. The authors suggested that the two edingtonite phases are a consequence of different nucleation phenomena and not different physico-chemical conditions. Similarly, the occurrence of "ordered" and "disordered" thomsonite in the same sample suggests that the two different forms would be controlled by different nucleation phenomena, rather than by different P/T genetic conditions.

REFERENCES CITED

Alberti, A., Vezzalini, G., and Tazzoli, V. (1981) Thomsonite: A detailed refinement with cross checking by crystal energy calculations. Zeolites, 1, 91–97.

Amirov, S.T., Asratkulu, M.O., Mamedov, Kh.S., and Belov, N.V. (1972) The crystal structure of zeolite-gonnardite Na$_2$Ca(Al$_2$Si$_3$O$_{10}$)$_2$(H$_2$O)$_6$. Doklady Akademii Nauk SSSR, 203, 1299–1301.

Amirov, S.T., Amiraslanov, I.R., Usubaliev, B.T., and Mamedov, Kh.S. (1978) Refinement of the crystal structure and symmetry of the zeolite-thomsonite. Azerbaidzhanskii Khimicheskii Zhurnal, 120–127.

Armbruster, T. and Gunter, M.E. (2001) Crystal structures of natural zeolites. In D.L. Bish and D.W. Ming, Eds., Natural Zeolites: Occurrence, properties, application, 45, p. 1–57. Reviews in Mineralogy and Geochemistry, Mineralogical Society of America and Geochemical Society, Chantilly, Virginia.

Artioli, G. and Galli, E. (1999) Gonnardite: Re-examination of holotype material and discreditation of tetranatrolite. American Mineralogist, 84, 1445–1450.

Arnò, V., Principe, C., Rosi, M., Santacroce, R., Sbrana, A., and Sheridan, M.F. (1987) Eruptive history. In R. Santacroce, Ed., Somma-Vesuvius. 114—Progetto Finalizzato Geodinamica, Quaderni de "La Ricerca Scientifica," Monografie finali, 8, p. 53–103. Consiglio Nazionale della Ricerca, Rome, Italy.

Baerlocher, Ch., Meier, W.M., and Olson, D.H. (2001) Atlas of Zeolite Framework Types, 5th edition, 302 p. Elsevier, Amsterdam.

Bernasconi, A., Bruni, P., Gorla, L., Principe, C., and Sbrana, A. (1981) Risultati preliminari dell'esplorazione geotermica profonda nell'area vulcanica del Somma-Vesuvio. Rendiconti della Societá Geologica Italiana, 4, 237–240.

Brocchini, F., Principe, C., Castradori, D., Laurenzi, M.A., and Gorla, L. (2001) Quaternary evolution of the southern sector of the Campanian plain and early Somma-Vesuvius activity: Insights from the Trecase well. Mineralogy and Petrology, 73, 67–91.

Chiari, G. and Ferraris, G. (1982) The water molecules in crystalline hydrates studied by neutron diffraction. Acta Crystallographica, B38, 2331–2341.

Coombs, D.S., Alberti, A., Armbruster, T., Artioli, G., Colella, C., Grice, J.D., Galli, E., Liebau, F., Minato, H., Nikel, E.H., Passaglia, E., Peacor, D.R., Quartieri, S., Rinaldi, R., Ross, M., Sheppard, R.A., Tillmans, E., and Vezzalini, G. (1997)

Recommended nomenclature for zeolite minerals: Report of the subcommittee on zeolite of the International Mineralogical Association Commission on New Minerals and Mineral Names. Canadian Mineralogist, 35, 1571–1606.

Della Ventura, G., Gatta, G.D., Redhammer, G.J., Bellatreccia, F., Loose, A., and Parodi, G.C. (2009) Single-crystal polarized FTIR spectroscopy and neutron diffraction refinement of cancrinite. Physics and Chemistry of Minerals, 36, 193–206, DOI: 10.1007/s00269-008-0269-8.

Dutta, P.K. and Del Barco, B. (1985) Structure-sensitive Raman bands in hydrated zeolite A. Journal of the Chemical Society, Chemical Communications, 1297–1299.

Dutta, P.K. and Puri, M. (1987) Synthesis and structure of zeolite ZSM-5: A Raman spectroscopic study. Journal of Physical Chemistry, 91, 4329–4333.

Evans Jr., H.T., Konnert, J.A., and Ross, M. (2000) The crystal structure of tetranatrolite from Mont Saint-Hilaire, Québec, and its chemical and structural relationship to paranatrolite and gonnardite. American Mineralogist, 85, 1008–1015.

Farrugia, L.J. (1999) WinGX suite for small-molecule single-crystal crystallography. Journal of Applied Crystallography, 32, 837–838.

Gatta, G.D. (2005) A comparative study of fibrous zeolites under pressure. European Journal of Mineralogy, 17, 411–421.

——— (2008) Does porous mean soft? On the elastic behaviour and structural evolution of zeolites under pressure. Zeitschrift für Kristallographie, 223, 160–170.

Gatta, G.D. and Boffa Ballaran, T. (2004) New insight into the crystal structure of orthorhombic edingtonite: Evidence for a split Ba site. Mineralogical Magazine, 68, 167–175.

Gatta, G.D., Boffa Ballaran, T., Comodi, P., and Zanazzi, P.F. (2004a) Isothermal equation of state and compressional behaviour of tetragonal edingtonite. American Mineralogist, 89, 633–639.

——— (2004b) Comparative compressibility and equation of state of orthorhombic and tetragonal edingtonite. Physics and Chemistry of Minerals, 31, 288–298.

Gatta, G.D., Rotiroti, N., McIntyre, G.J., Guastoni, A., and Nestola, F. (2008) New insights into the crystal chemistry of epididymite and eudidymite from Malosa, Malawi: A single-crystal neutron diffraction study. American Mineralogist, 93, 1158–1165.

Gatta, G.D., Cappelletti, P., Rotiroti, N., Slebodnick, C., and Rinaldi, R. (2009) New insights into the crystal structure and crystal chemistry of the zeolite phillipsite. American Mineralogist, 94, 190–199.

Gillet, P., Malézieux, J.M., and Itié, J.P. (1996) Phase changes and amorphization of zeolites at high pressure: the case of scolecite and mesolite. American Mineralogist, 81, 651–657.

Gottardi, G. and Galli, E. (1985) Natural Zeolites, 409 p. Springer-Verlag, Berlin.

Langella, A., Calcaterra, D., Cappelletti, P., Colella, A., d'Albora, M.P., Morra, V., and de Gennaro, M. (2009) Lava stones from Neapolitan volcanic districts in the architecture of Campania region, Italy. Environmental Earth Sciences, 59, 145–160, DOI: 10.1007/s12665-009-0012-x.

Mazzi, F., Larsen, A.O., Gottardi, G., and Galli, E. (1986) Gonnardite has the tetrahedral framework of natrolite: Experimental proof with a sample from Norway. Neues Jahrbuch für Mineralogie, Monatsheften, 5, 219–228.

Oxford Diffraction (2009) Xcalibur CCD system, CrysAlis Software system. Oxford Diffraction, Oxfordshire.

Passaglia, E. and Sheppard, R.A. (2001) The crystal chemistry of zeolites. In D.L. Bish and D.W. Ming, Eds., Natural Zeolites: Occurrence, properties, application, 45, p. 69–116. Reviews in Mineralogy and Geochemistry, Mineralogical Society of America and Geochemical Society, Chantilly, Virginia.

Peccerillo, A. (2001) Geochemical similarities between the Vesuvius, Phlegraean Fields and Stromboli Volcanoes: petrogenetic, geodynamic, and volcanological implications. Mineralogy and Petrology, 73, 93–105.

Pluth, J.J., Smith, J.V., and Kvick, Å. (1985) Neutron diffraction study of the zeolite thomsonite. Zeolites, 5, 74–80.

Ross, M., Flohr, M.J.K., and Ross, D.R. (1992) Crystalline solution series and order-disorder within the natrolite mineral group. American Mineralogist, 77, 685–703.

Rotiroti, N., Gatta, G.D., and Petrelli, M. (2008) New insight into the extra-framework content of zeolite levyne. Proceedings of the Annual Meeting of the Italian Association of Crystallography, Sestri Levante (Genoa, Italy), September 7–12, 2008.

Russo, M. (1999) Le zeoliti del Vesuvio. Bollettino dell'Associazione Italiana Zeoliti, 14, 12–22.

Russo, M. and Punzo, I. (2004) I Minerali del Somma-Vesuvio, 317 p. Associazione Micro-mineralogica Italiana, Cremona, Italy.

Santacroce, R. (1987) Somma-Vesuvius. Quaderni de "La Ricerca Scientifica," 114(8), 251 p. Consiglio Nazionale della Ricerca, Rome, Italy.

Sheldrick, G.M. (1997) SHELX-97. Programs for crystal structure determination and refinement. University of Göttingen, Germany.

Sheppard, R.A. and Hay, R.L. (2001) Formation of zeolites in open hydrologic systems. In D.L. Bish and D.W. Ming, Eds., Natural Zeolites: Occurrence, properties, application, 45, p. 261–275. Reviews in Mineralogy and Geochemistry, Mineralogical Society of America and Geochemical Society, Chantilly, Virginia.

Ståhl, K., Kvick, Å., and Smith, J.V. (1990) Thomsonite, a neutron diffraction study at 13 K. Acta Crystallographica, C46, 1370–1373.

Steiner, T. (1998) Opening and narrowing of the water H-O-H angle by hydrogen-bonding effects: Re-inspection of neutron diffraction data. Acta Crystallographica, B54, 464–470.

Taylor, W.H., Meek, C.A., and Jackson, W.W. (1933) The structures of fibrous zeolites. Zeitschrift für Kristallographie, Kristallgeometrie, Kristallphysik, Kristallchemie, 84, 373–398.

Wilson, A.J.C. and Prince, E. (1999) International Tables for Crystallography Volume C. Kluwer, Dordrecht.

Wopenka, B., Freeman, J.J., and Nikischer, T. (1998) Raman spectroscopic identification of fibrous natural zeolites. Applied Spectroscopy, 52, 54–63.